View metadata, citation and similar papers at core.ac.uk

brought to you by CORE

provided by NASA Technical Reports Server

NASA TECHNICAL NOTE

NASA TN D-8255

NASA TN D-8255 c.1

LOAN COPY: RETURN TO
AFWL TECHNICAL LIBRARY
KIRTLAND AFB, N.M.

TECH LIBRARY KAFB, NM
0133989

RESISTANCE OF NICKEL-CHROMIUM-ALUMINUM ALLOYS TO CYCLIC OXIDATION AT 1100° AND 1200° C

Charles A. Barrett and Carl E. Lowell

Lewis Research Center
Cleveland, Ohio 44135

NATIONAL AERONAUTICS AND SPACE ADMINISTRATION • WASHINGTON, D. C. • JUNE 1976

TECH LIBRARY KAFB, NM
0133989

1. Report No. NASA TN D-8255	2. Government Accession No.	3. Recipient's Catalog No.
4. Title and Subtitle RESISTANCE OF NICKEL-CHROMIUM-ALUMINUM ALLOYS TO CYCLIC OXIDATION AT 1100° AND 1200° C		5. Report Date June 1976 6. Performing Organization Code
7. Author(s) Charles A. Barrett and Carl E. Lowell		8. Performing Organization Report No. E-8615
9. Performing Organization Name and Address Lewis Research Center National Aeronautics and Space Administration Cleveland, Ohio 44135		10. Work Unit No. 505-01 11. Contract or Grant No.
12. Sponsoring Agency Name and Address National Aeronautics and Space Administration Washington, D.C. 20546		13. Type of Report and Period Covered Technical Note 14. Sponsoring Agency Code

15. Supplementary Notes

16. Abstract

Nickel-rich alloys in the Ni-Cr-Al system were evaluated for cyclic oxidation resistance in still air at 1100° and 1200° C. A first approximation oxidation attack parameter K_a was derived from specific weight change data involving both a scaling growth constant and a spalling constant. An estimating equation was derived with K_a as a function of the Cr and Al content by multiple linear regression and translated into contour ternary diagrams showing regions of minimum attack. An additional factor inferred from the regression analysis was that alloys melted in zirconia crucibles had significantly greater oxidation resistance than comparable alloys melted otherwise.

17. Key Words (Suggested by Author(s))
Cyclic oxidation; NiCrAl alloys; Oxidation attack parameter; Scale spalling; Regression analysis; Alloy optimization; Contour plotting; Zirconia effect

18. Distribution Statement
Unclassified - unlimited

19. Security Classif. (of this report)	20. Security Classif. (of this page)	21. No. of Pages	22. Price*
Unclassified	Unclassified	39	$4.00

* For sale by the National Technical Information Service, Springfield, Virginia 22161

RESISTANCE OF NICKEL-CHROMIUM-ALUMINUM ALLOYS TO CYCLIC OXIDATION AT 1100° AND 1200° C

by Charles A. Barrett and Carl E. Lowell

Lewis Research Center

SUMMARY

Nickel-rich alloys in the nickel-chromium-aluminum (Ni-Cr-Al) system were cyclically oxidized in still air for 500 1-hour heating cycles at 1100° C and 200 1-hour heating cycles at 1200° C. The specific sample weight-change data for each sample was then used to determine both a scaling growth constant k_1 and a spalling constant k_2 for each alloy using the regression equation $\Delta w/A = k_1^{1/2}t^{1/2} - k_2 t$ where t is time. These in turn were combined to form a first-approximation oxidation attack parameter K_a where $K_a = \left(k_1^{1/2} + 10\ k_2\right)$. Log K_a was then fitted to a fourth order regression equation as a function of the chromium and aluminum content at the two test temperatures. The derived estimating equations for log K_a are presented graphically as iso-attack contour lines on ternary phase diagrams at each temperature. At 1100° C compositions estimated to have the best cyclic oxidation resistances were Ni - 45 atomic percent Al and Ni - 30 atomic percent Cr - 20 atomic percent Al; at 1200° C compositions estimated to have the best cyclic oxidation resistances were Ni - 45 atomic percent Al and Ni - 35 atomic percent Cr - 15 atomic percent Al.

In general, good cyclic oxidation resistance is associated with aluminum sesquioxide (Al_2O_3) or nickel aluminate ($NiAl_2O_4$) formation. The analysis also indicated that alloys prepared by zirconia crucible melting, compared with other types of melting, showed that tramp zirconium pickup significantly improved the cyclic oxidation resistance. The nature of the improvement in oxidation due to this pickup, however, is not yet understood.

INTRODUCTION

In recent years many promising compositions have been identified in the nickel-chromium-aluminum (Ni-Cr-Al) system for use in applications requiring a high degree

of elevated-temperature oxidation resistance. Such applications have included both coatings for many types of alloys (ref. 1) and matrices for oxide dispersion-strengthened alloys (ref. 2). In spite of the wide use of such compositions, the only systematic investigation of the oxidation resistance of Ni-Cr-Al alloys has been done using isothermal oxidation resistance as the sole criterion (ref. 3). Aluminum sesquioxide (Al_2O_3) has been identified as the most desirable barrier to rapid oxidation. Therefore, much work has been aimed at oxide mapping to identify compositions that form Al_2O_3 exclusively. An example of the results of such mapping is shown in figure 1. From this work it is readily apparent that, as the amount of chromium is increased, the amount of aluminum necessary to form Al_2O_3 exclusively is reduced. Since high aluminum content alloys are known to be brittle, compositional development emphasis in this system has centered around low aluminum (10 to 20 at. %) and high chromium (15 to 25 at. %). This is true even in coatings which, in the past, have been based primarily on the β-phase (Ni to 50 at. % Al) alloy.

Contrary to the experimental oxidation work in this system, most, if not all, of the applications for these alloys require service of a cyclic nature. Since it is well established that cyclic exposure can drastically alter oxidation resistance (ref. 4), the work to be described in this report concerns cyclic oxidation. The purpose of this work was to survey nickel-rich alloys in Ni-Cr-Al system in order to identify compositions with optimum resistance to cyclic oxidation. Compositions were selected for study based on statistical procedures to get maximum information from a minimum number of alloys. The cyclic oxidation weight change data for each alloy were treated analytically to calculate a single constant, which is characteristic of the cyclic oxidation resistance of that alloy; that is, a first approximation oxidation attack parameter was obtained. This constant was then fitted to a polynomial equation that described it as a function of chromium and aluminum content.

MATERIALS

All of the alloys initially prepared for this program were vacuum melted in zirconia crucibles and cast in zirconia shell molds. Zirconium pickup of up to 0.6 weight percent was detected. Each mold consisted of a tree of ten 2.5- by 5.1- by 0.25-centimeter coupons, each with its own riser. For each coupon used the risers were removed and analyzed by atomic absorption for chromium and aluminum. Tables I and II give the chemistries determined for all alloys used in this work along with their nominal compositions.

The initial alloy series was chosen so that it would cover the region of most interest in a central composite star array (ref. 5) designed to give the maximum infor-

mation concerning changes of oxidation resistance with composition. The central composite array is shown graphically by the square data symbols in figure 2. Also shown are the actual compositions of both the initial series of alloys and the supplemental series of alloys. As can be seen, the initial series of compositions were close to the desired values, although alloys 2, 5, and 8 were recast to better approximate the desired chromium and aluminum levels.

Most of the supplemental alloys were obtained from previous programs (ref. 6) and were vacuum cast using zirconia molds and alumina crucibles. These alloys were cast into 1.9-centimeter-diameter, round bars. In addition, two other supplemental alloys were arc-melted ingots in copper molds especially for this program. These compositions are also shown in figure 2.

The compositions of all of these alloys are also shown in figure 3, a more familiar ternary plot which includes the phase boundaries as established by Taylor and Floyd (ref. 7).

After casting, the round bars were sliced into 0.2-centimeter-thick disks while the coupons were cut into 0.13- by 2.3- by 0.23-centimeter pieces. Each sample then had a hanger hole drilled and was glass-bead blasted. After cleaning, the samples were ready for testing.

Metallographic examination of the as-cast materials revealed four general types of structures. Figure 4(a) is a single-phase structure typical of γ-nickel solid solution found primarily in alloys 7 and 12, of $Ni_3Al(\gamma')$ found in alloys 14 to 17, and of $NiAl(\beta)$ found in alloys 18 to 21. Figure 4(b) shows the γ/γ' structure found in most nickel-base superalloys and alloys 3 and 9 of this program. Figure 4(c) represents the $\gamma' + \beta$ structure found in alloy 1. The final structure (fig. 4(d)) is found in alloys 2, 5, 6, and 8. It consists of a blocky structure of γ' and β with small particles of chromium solid solution (αCr) in the β.

PROCEDURES

Exposure and Postmortem Tests

The cyclic oxidation apparatus has been described in detail in reference 4. Sample dimensions were measured before testing. The thickness measurements in particular were precise to ±1 micrometer. Samples were thermally cycled to allow 1 hour in the furnace and a minimum of 40 minutes cooling in static air. The temperature profile is shown in figure 5. Samples reached the test temperature in less than 2 minutes after insertion into the furnace and cooled to ambient temperature in less than 20 minutes after removal from the furnace. Samples of each alloy were exposed for

500 cycles at 1100° C and 200 cycles at 1200° C. Specific weight change $\Delta w/A$ was determined at regular intervals throughout the test. At the conclusion of testing, samples were examined by X-ray diffraction and metallography. Metallographic analysis included thickness loss determination.

Mathematical Evaluation

The procedure used in the analysis of the specific weight change versus cyclic time data involves a series of steps using multiple linear regression. This procedure is described in detail in appendix A and is briefly summarized here as follows:

The change in $\Delta w/A$ with time t in the furnace (shown schematically in fig. 6) is fitted by least squares to equation (A1) using the method described in reference 8:

$$\frac{\Delta w}{A} = k_1^{1/2} t^{1/2} - k_2 t \pm \sigma \tag{A1}$$

where k_1 is the oxide growth constant analogous to the parabolic oxidation scaling constant, k_2 is an oxide spalling constant, and σ is the standard error of estimate. Then, by combining k_1 and k_2 a single first approximation oxidation attack parameter K_a is determined for each alloy:

$$K_a = k_1^{1/2} + 10\, k_2 \tag{A2a}$$

The number 10, an empirically determined weighting factor has been selected as the spall constant multiplier. (See appendix A.) A final multiple linear regression analysis up to the fourth order is then used to define the constants a and b_1 to b_{14} at each test temperature:

$$\log K_a = a + b_1 Cr + b_2 Al + b_3 AlCr + b_4 Cr^2 + b_5 Al^2 + b_6 CrAl^2 + b_7 AlCr^2 + b_8 Cr^3$$

$$+ b_9 Al^3 + b_{10} Cr^2 Al^2 + b_{11} Cr^3 Al + b_{12} CrAl^3 + b_{13} Cr^4 + b_{14} Al^4 \pm \sigma \tag{A6a}$$

where the b_i coefficients that are not significant to the 90 percent probability level are successively dropped and the equation recalculated.

These equations define the dependence of $\log K_a$ on composition.[1] Equation (A6a)

[1] $\log K_a$ was used instead of K_a as the independent variable to homogenize the error variance of small and large values of K_a.

can then be used to generate estimated attack contours at any level or levels of $\log K_a$ desired for mapping cyclic oxidation resistance.

RESULTS

Specific Weight Change

Values for $k_1^{1/2}$ and k_2 are given in tables III(a) and (b) for each sample oxidized. The table also includes the coefficient of variation R^2, which is the fraction of total variation explained by the regression equation, and the standard error of estimate σ - the error in estimating $\Delta w/A$ using the regression equation to help evaluate the degree of fit. Selected plots of $\Delta w/A$ against t are shown in figure 7 for a visual evaluation of the degree of fit.

The average values of K_a derived from the k_1 and k_2 values are shown in table IV for each alloy at 1100° and 1200° C. At 1100° C, K_a ranged from 0.09 to 103, and at 1200° C the range was from 0.27 to 153. The regression estimated equations derived for each temperature in terms of $\log K_a = f(Cr, Al)$ involved fourth order equations. As shown in equation (A6a), the fraction of explained variation (i.e., sum of squares) due to regression was increased significantly if a dummy variable was included (ref. 9) when alloys melted in zirconia crucibles were used. This difference in fit and the sign of the coefficient implied that traces of zirconium had a major effect on cyclic oxidation resistance. This difference is shown on table V, which indicates improvement in R^2 at both temperatures along its corresponding lower standard error of estimate.

The sets of estimated attack contours[2] generated from the regression estimating equations in terms of $\log K_a$ are shown in figures 8 and 9 for each temperature. The curves plotted are isoattack lines. Figures 8(a) and 9(a) show the curves for alloys melted in zirconia crucibles, and 8(b) and 9(b) represent alloys melted in alumina or in copper, water-cooled molds. As shown in table V, $\log K_a$ is lowered by a constant value of 1.48 at 1200° C and 0.67 at 1100° C because of the coefficient b_{15}. It should be remembered that the lower the $\log K_a$, the more oxidation resistant the alloy and that alloys with the same $\log K_a$ values are assumed to have the same oxidation resistance. Figure 8(a), for example, shows two areas of minimum attack, one centered near Ni-30Cr-20Al and the other at Ni-45Al. From these two regions the $\log K_a$

[2]The limiting contour values of $\log K_a = -1.25$ and -1.00 at 1100° and 1200° C, respectively, are derived from isothermal oxidation for Al_2O_3/aluminate spinel forming alloys (ref. 4).

values rise from -1.25 to -0.75 fairly gradually and then quite steeply into the nickel-rich γ region. Figure 8(b) is exactly the same contour map as 8(a) except it is greater by a fixed value of 0.67. Thus, when the same six contours are solved for the lower value, areas are more restricted. The same arguments hold for interpreting the contour maps at 1200° C, except that figure 9(b) is higher than 9(a) by a constant value of 1.48 (i.e., b_{15}). At 1200° C the two minimum areas are centered near Ni-35Cr-15Al and Ni-45Al, respectively.

The curves were compared at both temperatures to give generalized regions of estimated good, fair, and poor cyclic oxidation resistance in figure 10. Good cyclic oxidation resistance is estimated for two regions: one approximately at Ni-45Al and the other near Ni - 30 to 35 atomic percent Cr - 15 to 20 atomic percent Al. The poor region is mostly in the γ phase, nickel-rich end of the diagram with a hump at 15 to 25 percent Cr. The rest of the alloy system can be said to have fair cyclic oxidation resistance. These curves are defined based on values derived from the estimating equations for alloys melted in zirconia crucibles. The same regions would hold for the alloys prepared in other containers but the resistance would be poorer in each region.

X-Ray Diffraction

Unlike the oxides formed after isothermal oxidation in the work previously cited (ref. 3), few of the alloys cyclically tested in this work formed oxide layers consisting of Al_2O_3 exclusively. For this evaluation both the spalled and retained oxides were identified. Figure 11 summarized the X-ray diffraction results, which are substantially the same at both 1100° and 1200° C. Area I contains alloys whose oxides are predominately αAl_2O_3 and $NiAl_2O_4$. Area II contains alloys whose oxides are mostly NiO with $NiCr_2O_4$. Finally, area III and IV are dominated by NiO and Cr_2O_3, respectively.

Metallography

Figures 12 to 15 contain photomicrographs of a representative series of alloys after 500 cycles at 1100° C and 200 cycles at 1200° C. The same breakdown into types was used for their selection as was used in the selection of the as-cast micrographs. The single-phase alloy shows external scale formation, internal oxidation, and oxide penetration at 1100° C, but only external scale formation and internal oxidation at 1200° C (fig. 12).

The γ/γ' alloys (fig. 13) show external scale formation, oxide penetration, and a

zone depleted in γ' at both temperatures. The $\gamma' + \beta$ alloys (fig. 14) give similar results, that is, external scale, a depletion zone, and oxide penetration. Finally, the $\gamma' + \beta + \alpha$ alloy (fig. 15) has only a depletion zone and external oxidation, although in some cases oxide penetration was noted. Two other points of interest can be seen in figure 15: the presence of martensitic β (figs. 15(a) and (b)) and the absence of αCr after exposure at either temperature. Table VI details the modes of attack found in the alloys tested at both temperatures.

Change in Thickness

Detailed measurements of metal recession, depth of oxide penetration, extent of internal oxidation, and depletion zone thickness were made on the initial series of alloys tested at both temperatures. However, direct correlation was difficult to find between these measurements and the weight change data for alloys of differing microstructures because of the varying nature of the oxidation attack. Table VII shows the measured attack for the initial series of alloys after the 1200° C tests. Also listed is the calculated K_a for each sample as well as the final sample specific weight change after 200 hours. In general, the low K_a's and low sample-weight loss agree with the measured attack.

DISCUSSION

Specific Weight Change

Since the basis for the evaluation of cyclic oxidation attack is the equation combining $\Delta w/A$, k_1, and k_2, the degree of fit and its implications are important. In general the fit is good, but two reservations need pointing out. First, discontinuous data are being fit to a continuous function. The implication of the $\Delta w/A$ equation is that spalling and scale formation are happening concurrently when they are actually alternating phenomena. Second, unlike the paralinear equation developed in reference 10, k_1 and k_2 are not directly relatable to fundamental oxidation constants. However, as appendix B details they can ultimately be related by the K_a constant to an effective sample thickness change. This is based on the specific amount of metal consumed and converted to oxide up to a given time. Arguments are presented in appendix B justifying K_a as a reasonable first approximation oxidation attack parameter. This approach seems particularly promising for systems like Ni-Cr-Al where oxidation and spalling appear relatively uniform.

Based on the replication error of $\log K_a$, the overall experimental error for these Ni-Cr-Al alloys was about 20 percent at each temperature. The final fourth-order estimating equations had standard error of estimates equivalent to about 80 percent of K_a. For example, $\log K_a = 2.000 \pm 0.264692$ converts to $K_a = 100$, with upper and lower limits of 183.95 and 54.36. Considering that K_a is representing a complex reaction over a complex multiphase alloy system, the parameter seems to have performed satisfactorily at least as a relative rating indicator. Since the primary goal of this study was to locate compositions where optimum oxidation resistance might be achieved, the work can be considered successful. However, to substantiate these findings by the exact determinations of cyclic oxidation resistance, their relative importance established, more specific criteria of the extent of attack would be needed (Δt, oxide penetration, depletion zone depth) and samples of the compositions in question would have to be tested, particularly in the extreme parts of the diagram.

A surprising result of this investigation was the effect of zirconium pickup, which results from melting the samples in zirconia crucibles, on oxidation resistance. In terms of the attack parameter, melting in zirconia caused, on the average, an increase of about a factor of 10 in cyclic oxidation resistance at both test temperatures. For example, the paralinear analysis technique described in appendix B predicts that alloys forming $NiAl_2O_4$ with $\log K_a = -0.5$ (i.e., with zirconia melting) would consume roughly 100 micrometers of metal in 2900 hours while a comparable alloy with $\log K_a = +0.5$ (i.e., no zirconia melting) would consume a comparable amount in approximately 180 hours.

The reasons for the trace pickup of zirconium causing this effect are still being explored.

There are two points of interest about the position of the best compositions. First, the alloys with the greatest resistance to cyclic oxidation do not necessarily form Al_2O_3 exclusively but may also form some $NiAl_2O_4$ in the scale. Thus, the appearance of this nickel aluminate spinel does not signify less resistance. The second and more important point is that one of the two estimated best compositions lies near 30 to 35 atomic percent chromium and 15 to 20 atomic percent aluminum. These compositions would have large amounts of αCr (ref. 11), a phase whose coefficient of thermal expansion has been identified as being the closest to the Al_2O_3, the primary surface oxide phase in the Ni-Cr-Al system. Thus, as suggested in reference 11, if a mismatch in the coefficient of thermal expansion is important in spalling, the low values for αCr may account for the predicted high degree of cyclic oxidation resistance.

CONCLUDING REMARKS

The method of data handling used here seems to be valid for this type of first approximation predictive analysis. More work is necessary on compositions estimated to be superior and on establishing better criteria for oxidation attack than weight change alone. It appears that alloys of higher Cr levels than typically used may have promise. Also, as other aspects of the overall Lewis Ni-Cr-Al optimization program are completed, trade-offs may be necessary to find the alloy with the best balance of cyclic oxidation resistance, hot corrosion resistance, tensile properties, ductility, and strategic element content. However, it is quite likely that the higher Cr content alloys predicted to have good oxidation resistance have good hot corrosion resistance as well.

SUMMARY OF RESULTS

Alloys in the nickel-chromium-aluminum (Ni-Cr-Al) system were cyclically oxidized in air at 1100° C for 500 hours and 1200° C for 200 hours. The data were analytically and statistically treated to obtain first approximation oxidation attack parameters and subsequent estimated attack-composition contours. The results of this work may be summarized as follows:

1. At 1100° C compositions estimated to have the best cyclic oxidation weight change resistance were Ni - 45 atomic percent Al and Ni - 30 atomic percent Cr - 20 atomic percent Al. At 1200° C compositions estimated to have the best cyclic oxidation weight change resistance were Ni - 45 atomic percent Al and Ni - 35 atomic percent Cr - 15 atomic percent Al.

2. Alloys melted in zirconia crucibles have significantly improved cyclic oxidation resistance due to zirconium or zirconium oxide pickup.

3. Scales of α-aluminum sesquioxide and α-aluminum sesquioxide plus nickel aluminate are both associated with the best cyclic oxidation resistance.

Lewis Research Center,
National Aeronautics and Space Administration,
Cleveland, Ohio, March 23, 1976,
505-01.

SAMPLE CALCULATIONS TO DERIVE COMPOSITIONAL CONTOUR MAPS OF OXIDATION ATTACK

The calculations involved in deriving the final contour plots used a series of computational steps that will be described for one alloy set of three samples tested at 1200^{o} C in three separate runs. These stepwise calculations are as follows:

(1) Calculation of the oxidation constants k_1 and k_2 to describe the sample weight change process by regression analysis - Table VIII lists each of the observed specific weight change values at the test times involved along with the calculated points for three individually calculated alloy 1 samples based on the model equation

$$\frac{W}{A} = k_1^{1/2} t^{1/2} - k_2 t \pm \sigma \qquad \text{(A1)}$$

The derived constants $k_1^{1/2}$ and k_2 are also listed along the standard error of estimate (i. e., σ) and the coefficient of variation R^2, which gives the fraction of explained variation due to the regression equation. The level of significance for the $k_1^{1/2}$ and k_2 regression coefficients are usually set at 90 percent. If they are not significant at this level, they are automatically dropped and the equation is recalculated. For example, if the process were parabolic with no weight loss due to spalling, the k_2 term would drop out. As expected, since most of the samples eventually lose weight, the sign before k_2 is negative in the regression analyses.

The sample curves in figure 7 compare typical curves based on the derived $k_1^{1/2}$ and k_2 values with data. In most cases the model equation appears satisfactory as a first approximation.

(2) Conversion of the descriptive oxidation constants to a single attack parameter - Because the oxidation behavior is to be optimized over a composition range, it is necessary to develop a single parameter directly proportional to oxidation attack. Ideally, this should be analagous to a tensile strength or rupture life or some other alloy property that can be directly measured. In cyclic oxidation there is no readily observable parameter, although a measured thickness change at a given test time would be excellent if it could be easily measured and normalized with time. This has not proven practicable as yet. As an alternative it seemed reasonable that, once a weight change curve in cyclic oxidation seemed stable with time, combining the two oxidation constants in a dimensionally consistent way would give a first approximation single-attack parameter needed to optimize over the composition range. On this basis the attack

parameter was defined as

$$K_a = k_1^{1/2} + ck_2 \tag{A2}$$

where c is a simple numerical constant in this case equal to 10. The units on K_a therefore are milligrams per square centimeter, and k_2 in this case is a positive number defined as the loss rate (in mg/cm^2). Obviously, as k_1 and k_2 increase, the value of K_a increases also. If either k_1 or k_2 drops out of equation (A1) as being nonsignificant, the remaining constant can still be used in defining K_a. For example, if $k_1 = 0.1$ and $k_2 = 0.01$, then $K_a = 0.2$. In this context this is equivalent to straight parabolic oxidation with $k_1 = 0.2$ and $k_2 \sim 0$. Or, if the weight loss curves were linear as appears in some burner rig tests (ref. 12), a $k_2 = 0.02$ is equivalent. This in theory puts all types of oxidation tests on the same basis, at least as a first approximation.

Obviously the form of K_a could be much more complicated since, particularly in a spalling case, k_1 and k_2 as well as c could vary with time. Showing the validity of the simpler equation (A2), at least for this series of alloys, was attempted and is described in appendix B.

(3) Use of the oxidation attack parameter to estimate the optimal composition for minimal cyclic oxidation attack - The next step is to estimate K_a over the atomic percent ternary region of interest as a function of the aluminum and chromium content. Multiple linear regression was used with a polynomial model. Because the range of K_a's is so large, the relative, rather than the absolute, error of K_a is assumed to be constant. This is done in the estimating equation by transforming K_a to $\log K_a$ and is termed homogenizing the error variance. The polynomial model equations in terms of two variables, $X_1 = Cr$ and $X_2 = Al$ are

First order:

$$\log K_a = a + b_1X_1 + b_2X_2 \pm \sigma \tag{A3}$$

Second order:

$$\log K_a = a + b_1X_1 + b_2X_2 + b_3X_1^2 + b_4X_2^2 + b_5X_1X_2 \pm \sigma \tag{A4}$$

Third order:

$$\log K_a = a + b_1X_1 + b_2X_2 + b_3X_1^2 + b_4X_2^2 + b_5X_1X_2 + b_6X_1^3 + b_7X_2^3 + b_8X_1^2X_2 + b_9X_1X_2^2 \pm \sigma \quad \text{(A5)}$$

Fourth order:

$$\log K_a = a + b_1X_1 + b_2X_2 + b_3X_1^2 + b_4X_2^2 + b_5X_1X_2 + b_6X_1^3 + b_7X_2^3 + b_8X_1^2X_2 + b_9X_1X_2^2 + b_{10}X_1^4 + b_{12}X_3^3X_1 + b_{13}X_3X_1^3 + b_{14}X_1^2X_2^2 \pm \sigma \quad \text{(A6)}$$

Generally, the approach is to start at equation (A3) and go higher if necessary but rarely beyond the fourth power fit (eq. (A6)) (ref. 9).

Since this is effectively a topographic mapping of the Ni-50Cr-50Al region, the more complex the response (i. e., terrain) the more complex the equation to describe it. The problem of a complex equation like (A6) is that it may give nonsense values at locations away from the data points. Thus, when a final reasonable equation is generated, its predicted y values were plotted not only at the respective data point sets (32 at each temperature) but also at the various 5-atomic percent grid intersections on the ternary along with each standard deviation. These standard deviations will vary from a minimum, based on the derived standard error of estimate, to larger values - depending on how far the composition is from the actual data points. Thus, the strategy is to build the model from equations (A3) to (A6), again setting the significance level for a coefficient at the 90 percent probability level.

This progressive approach is summarized in table IX. After this analysis was completed, it was found that adding a dummy variable to account for the effect of zirconia crucible melting significantly improved R^2 and lowered the standard error of estimate of the regression equations. On this basis the hypothesis that the zirconia melting significantly altered the oxidation behavior of Ni-Cr-Al alloys at 1100° and 1200° C was accepted. Since the coefficients at both temperatures are negative, it is inferred that the oxidation behavior is improved.

Once the final estimating equations are selected they may be too complex to readily interpret. Computer programs, however, are available to convert the equations into iso-y values, which are then plotted as topographic contour maps. These summarize the cyclic oxidation behavior showing the composition regions of high- and low-oxidation resistance and the optional design compositions as well.

APPENDIX B

RELATION OF THE ATTACK PARAMETER K_a TO THE TOTAL OXIDATION PROCESS INVOLVING BOTH SCALE GROWTH AND SCALE SPALL

It has been shown that oxidation involving both scale growth and scale spall can be expressed in terms of specific sample weight change as

$$\frac{\Delta w}{A} = k_1^{1/2} t^{1/2} - k_2 t \tag{B1}$$

With the regression analysis of most of the alloys tested in this report, equation (B1) gives a good fit of the data. The fraction of variability R^2 explained by regression is well over 0.90.

Equation (B1) is also of the same form as the approximate paralinear equation as discussed in references 4 and 10. The equation in approximate paralinear form is

$$\frac{\Delta w}{A} = k_p^{1/2} t^{1/2} - k_\ell t \tag{B2}$$

Where k_p is the conventional parabolic rate constant $\left(\text{in } (\text{mg/cm}^2)^2/\text{hr}\right)$ and k_ℓ is a linear loss constant (in mg/cm^2). Reference 4 discusses this form of the equation and compares it with the exact paralinear solution of the $\Delta w/A$ as a function of time relationship. In the exact solution, however, the expression for $\Delta w/A$ at any time t is defined as

$$\frac{\Delta w}{A} = w_r - w_m \tag{B3}$$

Here, w_r is the specific weight of the scale retained on the alloy up to time t and w_m is the total amount of metal converted to oxide both retained and spalled (and/or vaporized) up to time t (both in mg/cm^2). In any corrosion process w_m is the key parameter because it represents the amount of corrosion (i.e., metal consumed). It is always positive and always increases with time. Usually, w_m is quite difficult to measure, although the computer program described in reference 10 allows simple $\Delta w/A$ input data at two times with a known oxide to generate the complete $\Delta w/A$, w_m, and w_r values as functions of any desired times.

Thus, the strategy was to attempt to link equation (B1) to equation (B3) in some way. Therefore, equation (B1) was collapsed into a single parameter form:

$$K_a = \left(k_1^{1/2} + ck_2\right) \tag{B4}$$

where this equation is independent of time and whose values are in the units milligram per square centimeter per hour. Next, equation (B1) is solved for the zero-crossover time value such that at $\Delta w/A = 0$

$$t_{0\text{-cross}} = \frac{\left(k_1^{1/2}\right)^2}{k_2^2}$$

Thus two paired sets of specific weight changes and times are available from the calculated regression curve. These paired sets are then used as input in the parabolic computer program (termed COREST) in reference 10, assuming that $NiAl_2O_4$ is the major forming oxide. The computer output includes $\Delta w/A$, w_r, and, more importantly, w_m values as functions of time. Table X lists the $\Delta w/A$ values for three alloy 1 samples tested at 1200° C presented in table VIII. The match is quite close. The w_m values are also available as a function of time and are a direct measure of the corrosion. To further convert the w_m values to effective thickness loss, the w_m values are divided by the weighted average metallic density of nickel and aluminum in $NiAl_2O_4$. To test the validity of the attack parameter K_a as a link between equations (B1) and (B3), a series of least squares correlations was run of the form

$$\log \Delta t = a + b_1 \log\left(k_1^{1/2} + ck_2\right) \tag{B6}$$

(where Δt is the thickness change from one side in μm) for a series of c values ranging from 1 to 500. The $k_1^{1/2}$ and k_2 values were determined for the NiCrAl alloys 1 to 9 tested at 1200° C, 57 in all including replicates. Good straight line fits were obtained particularly for c values between 10 and 15. For this reason $c = 10$ was used in equation (B4). Figure 16 shows this relationship for $c = 10$ and shows the good linear association. This approach was carried further when the effective thickness loss was calculated by COREST for the same alloys, but this time for a whole range of times from 100 to 100 000 hours. The resulting regression estimating equation was fairly simple and is shown plotted on figure 17 for three values of $\log K_a$. This plot shows for example that a $NiAl_2O_4$ forming alloy with a $k_1 = 0.5$ and $k_2 = 0.05$ has a $K_a = (0.5 + 10 \times 0.05) = 1$. The log of $K_a = 0$, so that at 1000 hours approximately 135 micrometers of the alloy is consumed from one side.

The resulting estimating equation, with an $R^2 = 0.974$, is

$$\log \Delta \text{ thickness} = -0.489205 + 1.051488 (\log K_a) + 0.871487 (\log t) \pm 0.159403 \tag{B7}$$

This whole relationship was based on data generated at 1200° C for 200 1-hour cycles. If equation (B7) could be used to estimate attack on the 1100° C tested alloys, then confidence in the whole approach would be increased. Two alloys were chosen from the NiCrAl group: alloy 7 with a fairly high degree of attack and alloy 2a with an apparently low overall degree of attack.

Both values were calculated from equation (B7) along with their standard errors of estimate ranges. These are shown by the circular data points and error bands in figure 17. Also, the k_1 and k_2 values were used to calculate the zero net weight crossover time value and inputed into COREST along with the least squared estimated 500-hour value. The values obtained at 500 hours are shown in the shaded squares. Finally, we attempted to measure the thickness change in the two samples, accepting the difficulties described earlier. For alloy 2 the triangular point of 15 micrometers represents loss on one side, but the additional 20-micrometer depletion zone is not included. For alloy 7 the attack from one side includes both the metal loss and the wormy attack zone totaling 70 micrometers. The additional sparse internal oxidation is not included.

Thus the results, particularly for this alloy system, seem quite consistent, and K_a seems a valid first approximation attack parameter to characterize oxidation behavior. Its application to other alloy systems remains to be explored.

REFERENCES

1. Felten, E. J.; Strangman, T. E.; and Ulion, N. E.: Coatings for Directional Eutectics. (PWA-5091, Pratt and Whitney Aircraft; NAS3-16792) NASA CR-134735, 1974.

2. Timbres, Donald H.; Norris, L. F.; and Clegg, Maurice A.: Improvement of the Oxidation Resistance of Dispersion Strengthened Nickel-Chromium Alloys. Sherritt Gordon Mines, Ltd. (AD-748266; AFML-TR-72-50), 1972.

3. Wallwork, G. R.; and Hed, A. Z.: Some Limiting Factors in the Use of Alloys at High Temperatures. Oxidation of Metals, vol. 3, no. 2, Mar. 1971, pp. 171-184.

4. Barrett, Charles A.; and Lowell, Carl E.: Comparison of Isothermal and Cyclic Oxidation Behavior of 25 Commercial Sheet Alloys at 1150° C. Oxidation of Metals, vol. 9, no. 4, 1975, pp. 307-355.

5. Leone, Fred C.; and Johnson, Normal L.: Statistics and Experimental Design in Engineering and the Physical Sciences. Vol. 2, John Wiley & Sons, Inc., 1964.

6. Santoro, Gilbert J.; Deadmore, Daniel L.; and Lowell, Carl E.: Oxidation of Alloys in the Nickel-Aluminum System with Third Element Additions of Chromium, Silicon, and Titanium at 1100° C. NASA TN D-6414, 1971.

7. Taylor, A.; and Floyd, R. W.: The Constitution of Nickel-Rich Alloys of the Nickel-Chromium-Aluminum System. J. Inst. Met., vol. 81, 1952-53, pp. 451-464.

8. Sidik, Steven M.: An Improved Multiple Linear Regression and Data Analysis Computer Program Package. NASA TN D-6770, 1972.

9. Draper, Norman R.; and Smith, H.: Applied Regression Analysis. John Wiley & Sons, Inc., 1967, pp. 134-142.

10. Barrett, Charles A.; and Presler, Alden F.: COREST - A Fortran Computer Program to Analyze Paralinear Oxidation Behavior and its Application to Chromic Oxide Forming Alloys. NASA TN D-8132, 1975.

11. Lowell, Carl E.; Garlick, Ralph G.; and Henry, Bert: Thermal Expansion in the Ni-Cr-Al and Co-Cr-Al Systems to 1200° C. NASA TM X-3268, 1975.

12. Johnston, James R.; and Ashbrook, Richard L.: Effect of Cyclic Conditions on the Dynamic Oxidation of Gas Turbine Superalloys. NASA TN D-7614, 1974.

TABLE I. - CHEMISTRY OF INITIAL CASTINGS

Casting	As-cast composition, at. %			
	Nominal		Actual	
	Cr	Al	Cr	Al
1	16	18	15.98	17.54
2a	13	24	11.50	25.58
[a]2b	13	24	12.44	22.72
3	13	12	13.69	12.07
4	19	12	18.41	11.06
5a	16	30	14.25	23.65
[a]5b	16	30	16.81	29.19
6a	19	24	19.15	24.16
[b]6b	19	24	19.19	24.24
7	16	6	15.81	5.77
8a	22	18	18.87	26.99
[a]8b	22	18	20.84	16.52
9	10	18	9.73	17.18

[a]Recast for better match with nominal position.

[b]Recast for additional samples.

TABLE II. - CHEMISTRY OF SUPPLEMENTAL CASTINGS

[All samples are rectangular coupons except for disk samples melted in Al_2O_3 crucibles.]

Casting	As-cast composition, at. %			
	Nominal		Actual	
	Cr	Al	Cr	Al
10	20	0	19.87	0
11	40	0	38.70	0
12	10	0	10.49	0
[a]13	0	40	0	41.78
[b]14	0	25	0	24.9
[b]15	1	24	.78	24.5
[b]16	3	22	2.90	22.6
[b]17	10	15	9.98	15.73
[b]18	0	50	0	50.5
[b]19	1	49	1.1	48.8
[b]20	3	47	2.6	47.6
[b]21	10	40	10.3	39.1
[b]22	3	7	2.80	7.10
[b]23	1	9	1.20	8.90
24	16	10	16.30	10.16
[b]25	38	10	37.41	9.74
[a]26	30	20	29.30	19.32

[a]Arc melted ingots in copper molds.

[b]Castings were melted in Al_2O_3 crucibles and poured into 1.9-cm-diam Al_2O_3 molds.

TABLE III. - CYCLIC OXIDATION CONSTANTS

[Model equation: $\Delta W/A = k_1^{1/2} t^{1/2} - k_2 t \pm \sigma$; from multiple linear regression.]

(a) Initial series

Alloy	Actual alloy composition, at. %		Test temperature, °C									
			1100					1200				
	Cr	Al	Test time, hr	Square root of oxide growth constant, $k_1^{1/2}$, $\frac{mg/cm^2}{hr}$	Oxide spalling constant, k_2, $\frac{mg/cm^2}{hr}$	Coefficient of variation,[a] R^2	Standard error of estimate, σ, mg/cm^2	Test time, hr	Square root of oxide growth constant, $k_1^{1/2}$, $\frac{mg/cm^2}{hr}$	Oxide spalling constant, k_2, $\frac{mg/cm^2}{hr}$	Coefficient of variation,[a] R^2	Standard error of estimate, σ, mg/cm^2
1	15.98	17.54	500	0.0893	0.00510	0.978	0.05	200	0.280	0.0361	0.996	0.11
				.0960	.00559	.991	.04		.190	.0329	.998	.09
				.0788	.00413	.977	.05		.296	.0345	.992	.13
2a	11.50	25.58		.1036	.00823	.972	.12		.334	.0470	.998	.10
				.0882	.00816	.995	.06		.283	.0273	.926	.22
				.1064	.00734	.981	.08		.160	.0418	.999	.12
				------	-------	-----	----		.354	.0510	.999	[b].11
				------	-------	-----	----		.104	.0402	.999	[b].14
2b	12.44	22.72		.1315	.00643	.980	.08		.483	.0340	.968	.21
3	13.19	12.07		.1019	.00801	.994	.05		.247	.0272	.994	.08
				.1092	.00723	.992	.05		.299	.0227	.990	.07
				.1013	.00628	.991	.04		.181	.0246	.987	.15
				------	-------	-----	----		.137	.0149	.893	[b].19
				------	-------	-----	----		.164	.0290	.997	[b].10
4	18.41	11.06		.3329	.01688	.822	.63		4.846	.5538	.978	3.35
				.6040	.04302	.897	1.13		4.357	.6834	.939	3.78
				.5437	.03323	.840	1.01		3.109	.4487	.889	2.92
5a	14.35	23.65		.0996	.00219	.998	.04		.297	.0223	.993	.06
				.1101	.00203	.998	.05		.286	.0264	.992	.06
				.1079	.00222	.997	.05		.293	.0241	.991	.06
				------	-------	-----	----		.228	.0218	.985	.07
5b	16.81	29.19		.1881	(c)	.999	.09		.657	.0335	.991	.29
6a	19.15	24.16		.0850	.00523	.982	.05		.076	.0293	.999	.10
				.0891	.00596	.972	.07		(c)	.0327	.997	.23
				.0734	.00412	.988	.06		.187	.0271	.997	.09
6b	19.19	24.24		.0784	.00585	.948	.11		.021	.0311	.990	.10
				.0923	.00859	.991	.09		.058	.0258	.998	.12
7	15.81	5.77		.6801	.04413	.761	1.77		2.346	.3303	.941	4.52
				.5555	.03413	.811	1.15		1.624	.2733	.992	.59
8a	18.87	26.99		.0631	.00591	.983	.08		.240	.0227	.974	.10
				.0695	.00689	.992	.07		.147	.0280	.995	.15
				------	-------	-----	----		.189	.0235	.999	[b].04
				------	-------	-----	----		.179	.0273		[b].04
8b	20.84	16.52		.0124	.00726	.998	.06		.032	.0249		.07
				.0159	.00737	.999	.06		.016	.0241		.08
9	9.73	17.18		.0960	.00432	.977	.05		.269	.0250	.770	.37
				.1135	.00524	.977	.08		.214	.0195	.859	.21
				------	-------	-----	----		.080	.00321	.812	.22

[a]Ratio of explained variability to total variability.

[b]Samples tested as replicates within a given run.

[c]Value obtained and dropped - insignificant.

TABLE III. - Concluded.

[Model equation: $\Delta W/A = k_1^{1/2}t^{1/2} - k_2t \pm \sigma$; from multiple linear regression.]

(b) Supplemental castings

Alloy	Actual alloy composition, at. %		Test temperature, °C									
			1100					1200				
	Cr	Al	Test time, hr	Square root of oxide growth constant, $k_1^{1/2}$, $\frac{mg/cm^2}{hr}$	Oxide spalling constant, k_2, $\frac{mg/cm^2}{hr}$	Coefficient of variation,[a] R^2	Standard error of estimate, σ, mg/cm^2	Test time, hr	Square root of oxide growth constant, $k_1^{1/2}$, $\frac{mg/cm^2}{hr}$	Oxide spalling constant, k_2, $\frac{mg/cm^2}{hr}$	Coefficient of variation,[a] R^2	Standard error of estimate, σ, mg/cm^2
10	19.87	0	100	8.3364	2.80816	0.999	10.62	50	(c)	7.2520	0.996	15.57
				8.2680	2.77597	.999	3.19		(c)	7.0618	.989	24.27
11	38.70	0		(c)	.06336	.986	.42		0.304	.1931	.999	.15
				(c)	.06329	.984	.41		.289	.2001	.999	.12
12	10.49	0	55	(c)	10.00134	.971	63.29	45	(c)	14.0823	.963	75.88
			55	(c)	10.51662	.974	62.65	45	(c)	16.3706	.957	70.85
13	0	41.78	1373	.0790	.00256	.851	.18	160	.340	.0815	.999	.09
			500	.0610	.00216	.984	.28	---	------	-------	-----	------
14	0	24.9	[d]100	.3092	.05068	.971	.21	100	.579	.2510	.998	.60
15	.78	24.5		.2467	.05387	.991	.18	100	(c)	.2850	.997	.99
16	2.90	22.6		.3282	.12617	.998	.26	87	(c)	.3941	.992	2.24
				------	--------	-----	------	100	(c)	.4373	.993	2.19
17	9.98	15.73		1.3440	.37477	.998	.58		1.074	1.0487	.999	[b]1.34
				------	--------	-----	------		.630	.9754	.990	[b]1.90
18	.78	24.5		------	--------	-----	------		.107	.2772	.999	[b].25
				------	--------	-----	------		.047	.2538	.999	[b].22
19	0	50.5		.0520	.00411	.922	.05	200	.333	.0430	.993	.16
20	1.1	48.8		.0195	(c)	.759	.10	100	.367	.0771	.993	.20
21	2.6	47.6		.5173	.06850	.948	.25	100	1.060	.2651	.999	.21
22	10.3	39.1		1.091	.114	.954	.60	25	3.324	.5023	.979	.90
			100	.8791	(c)	.967	1.20	---	------	-------	-----	------
23	2.8	7.10	100	(c)	4.65497	.997	[b]16.15	45	(c)	10.2317	.997	[b]15.93
			100	(c)	4.55896	.995	[b]20.41	45	(c)	10.2220	.995	[b]20.87
			----	------	--------	-----	------	45	(c)	9.9666	.996	[b]17.75
24	1.2	8.90	500	4.4907	.60392	.957	[b]16.77	60	10.343	2.5349	.945	[b]9.84
			500	1.8714	.25203	.854	[b]13.69	60	11.241	3.1839	.972	[b]10.29
			----	------	--------	-----	------	60	9.649	2.9650	.962	[b]12.11
25	16.30	10.16	[e]100	.3118	.02068	.992	.11	200	3.207	.2901	.636	[b]6.72
			----	------	--------	-----	------		3.523	.3367	.760	[b]6.28
26	37.41	9.74	500	.4110	.05349	.983	[b].59		(c)	.1255	.999	[b].26
				.2333	.03211	.919	[b].87		(c)	.1400	.999	[b].60
27	29.30	19.32		(c)	.02714	.994	[b].54		(c)	.1154	.969	[b]2.56
				(c)	.03188	.994	[b].62		(c)	.1155	.958	[b]2.98

[a]Ratio of explained variability to total variability.

[b]Samples tested as replicates within a given run.

[c]Value obtained and dropped - insignificant.

[d]Ref. 6.

[e]After indicated time curve changes direction and sample gains weight to end of test.

TABLE IV. - AVERAGE CYCLIC OXIDATION CONSTANTS

(a) Initial castings; all melted in zirconia crucibles

Alloy	Actual composition, at.%		Attack parameter, $\overline{K}_a$	
			Temperature, °C	
	Cr	Al	1100	1200
1	15.98	17.54	0.14	0.60
2a	11.50	25.58	.18	.66
2b	12.44	22.72	.20	.82
3	13.69	12.07	.18	.44
4	18.41	11.06	.80	9.72
5	14.35	23.65	.13	.51
5b	16.81	29.19	.19	.99
6a	19.15	24.16	.13	.38
6b	19.19	24.24	.16	.32
7	15.81	5.77	1.01	5.01
8a	18.87	26.99	.13	.44
8b	20.84	16.52	.09	.27
9	9.73	17.18	.11	.35

(b) Supplemental series

Alloy	Actual composition, at.%		Attack parameter, $\overline{K}_a$		Melt container
			Temperature, °C		
	Cr	Al	1100	1200	(a)
10	19.87	0	36.19	71.57	1
11	38.7	0	.63	2.26	1
12	10.49	0	102.59	152.26	1
13	0	41.78	.09	1.16	0
14	0	24.9	.82	3.09	
15	.78	24.5	.79	2.77	
16	2.9	22.6	1.59	4.16	
17	9.98	15.73	5.09	10.96	
18	50.0	50.5	.09	.76	
19	1.1	48.8	.02	.81	
20	2.6	47.6	1.20	3.71	
21	10.3	39.1	2.24	8.35	
22	2.80	7.10	46.07	101.40	
23	1.20	8.90	7.46	39.36	
24	16.30	10.16	.52	6.50	1
25	37.41	9.74	.65	1.33	0
26	29.30	19.32	.30	1.15	0

[a]Zirconia crucibles, 1; other, 0.

TABLE V. - SUMMARY OF REGRESSION ANALYSIS OF POLYNOMIAL ESTIMATING EQUATION OF CYCLIC OXIDATION ATTACK PARAMETER

$$[\log K_a = b_0 + b_1 Cr + b_2 Al + \ldots + b_{14} Cr^2 Al^2 \pm \sigma.]$$

Temperature, °C	Number of data points (a)	Number of significant b's (b)	Coefficient of variation, R^2	Standard error of estimate, σ	Zirconium effect coefficient, b_{15} (c)
1200° C:					
No Zr effect	77	14 → 14	0.8285	0.3536	-------
Zr effect	77	15 → 12	.9038	.2628	-1.4777
1100° C:					
No Zr effect	66	14 → 9	0.8837	0.3349	-------
Zr effect	66	15 → 10	.9140	.2647	-0.6689

[a] Includes two twice weighted dummy K_a values at 45Cr-0Al and 50Cr-0Al, which were assumed equal to 38.7Cr-0Al values, to constrain the regression equation. In addition, the 50.5Al-0Cr and 41.78Al-0Cr were each weighted three times to balance the data in the extreme Al region.

[b] If b_i is not significant to 90 percent probability level, variable is dropped and equation successively recalculated.

[c] If Zr effect is included, $X_{15} = 1$; if not, $X_{15} = 0$.

TABLE VI. - MODES OF MICROSTRUCTURAL ATTACK

IN ADDITION TO OVERALL METAL LOSS

Alloy	Phases	Oxide penetration (a)	Depleted zone (a)	Internal oxidation or void formation (a)
7	γ	+	0	+
10	γ	0	↓	+
11	γ	0	↓	+
12	γ	0	↓	0
13	γ/γ'	+	↓	0
4	γ/γ'	+	↓	+
9	γ/γ'	+	+	0
14	γ'	0	+	↓
15	γ'	↓	+	↓
16	γ'	↓	+	↓
17	γ'	↓	+	↓
1	$\gamma' + \beta$	+	+	↓
18	β	0	0	↓
19	β	0	↓	↓
20	β	0	↓	↓
21	β	+	↓	↓
13	β	0	↓	↓
2a	$\gamma'^{+}/\beta^{+}/\alpha$	0	+	↓
2b	$\gamma'/\beta/\alpha$	0	+	↓
5a	$\gamma'/\beta/\alpha$	+	+	↓
5b	$\gamma'/\beta/\alpha$	+	+	↓
6	$\gamma'/\beta/\alpha$	0	+	↓
8a	$\gamma'/\beta/\alpha$	0	+	↓
8b	$\gamma'/\beta/\alpha$	0	+	↓

[a]Present, +; absent, 0.

TABLE VII. - MEASURED OXIDATION ATTACK

[Initial castings; 1-hr heating cycles; number of cycles, 200.]

Alloy	Average attack parameter, K_a	Observed weight change at end of test, $\Delta w/A$, mg/cm^2	Scale metal to scale metal loss, Δth, μm	Deepest penetration of oxide, μm	Depletion zone, μm	Internal oxidation, μm	Total maximum attack, μm
9	0.35	-0.49	0	128	534	---	534
		-.67	11	137	611	---	622
6a	.38	-4.64	27	---	71	---	98
		-2.67	29	---	54	---	83
		-6.21	54	---	70	---	124
3	.44	-.36	3	47	383	---	386
		-1.83	(a)	51	354	---	350
		-2.13	3	31	355	---	358
8a	.44	-3.32	44	---	24	---	68
		-1.23	13	---	51	---	64
5a	.51	-1.21	26	96	15	---	122
		-.69	30	91	12	---	121
		-.28	24	93	56	---	117
1	.60	-3.06	12	64	426	---	438
		-2.44	7	53	494	---	501
		-3.79	0	86	506	---	506
2a	.66	-4.71	51	---	62	---	113
		-6.02	22	---	110	---	132
		-1.67	80	---	26	---	106
7	5.01	-84.07	39	---	---	434	473
		-40.84	28	---	---	475	503
4	9.72	-43.80	15	Total	---	---	Total
		-46.25	19	Total	---	---	Total
		-60.73	11	Total	---	---	Total

[a]Slight growth of 4 μm.

TABLE VIII. - SPECIFIC WEIGHT CHANGE DATA OBSERVED AND CALCULATED FROM $\Delta w/A = k_1^{1/2} t^{1/2} - k_2 t$

[Alloy 1; three samples; test temperature, 1200° C.]

(a) Data

Time, hr	Run 1		Run 2		Run 3	
	$\Delta w/A_{obs}$	$\Delta w/A_{calc}$	$\Delta w/A_{obs}$	$\Delta w/A_{calc}$	$\Delta w/A_{obs}$	$\Delta w/A_{calc}$
1	0.30	0.26	0.28	0.24	0.24	0.16
15	.72	.63	.66	.54	.37	.24
30	.60	.59	.54	.45	.17	.06
45	.49	.44	.29	.25	-.22	-.20
60	.29	.23	.08	0	-.50	-.50
75	.03	-.02	-.21	-.28	-.75	-.82
90	-.21	-.29	-.64	-.60	-1.19	-1.15
100	-.49	-.49	-.89	-.81	-1.45	-1.38
115	-.94	-.79	-1.31	-1.15	-1.88	-1.74
130	-1.18	-1.11	-1.66	-1.50	-2.17	-2.10
145	-1.66	-1.43	-1.97	-1.88	-2.59	-2.47
160	-1.92	-1.77	-2.25	-2.24	-2.83	-2.85
175	-2.19	-2.12	-2.67	-2.62	-3.22	-3.23
190	-2.35	-2.47	-2.91	-3.01	-3.53	-3.62
200	-2.44	-2.71	-3.06	-3.27	-3.79	-3.88

(b) Constants used in calculations

Parameter	Run 1	Run 2	Run 3
Square root of growth constant, $k_1^{1/2}$	0.296315	0.279982	0.190190
Oxide spalling constant, k_2	0.0344995	0.0361278	0.0328545
Coefficient of variation, R^2	0.991729	0.996090	0.998451
Standard error of estimate, σ	0.13	0.11	0.09
Attack parameter, $K_a = (k_1 + 10\ k_2)$	0.641310	0.641260	0.518735
$\log K_a$	-0.192932	-0.192932	-0.285054
Average $\log K_a$ for alloy 1			-0.223639

TABLE IX. - POLYNOMIAL MULTIPLE LINEAR REGRESSION CURVE

[X_1 = Cr, X_2 = Al; $\log K_a = a_0 + b_1X_1 + b_2X_2 \ldots \pm \sigma$; rejection probability = 0.90.]

	Test temperature, °C					
	1100			1200		
	Number of variables, n					
	66 (a)			77 (b)		
	Final number of variables	Coefficient of variation, R^2	Standard error of estimate, σ	Final number of variables	Coefficient of variation, R^2	Standard error of estimate, σ
First order						
2 variables - X_1, X_2	2	0.526	0.580346	2	0.454	0.577746
3 variables - X_1, X_2, Zr	3	.634	.514124	3	.623	.482893
Second order						
5 variables - . . ., X_1^2, X_2^2, X_1X_2	5	.772	.412727	5	.723	.419590
6 variables - . . ., X_1^2, X_2^2, X_1X_2, Zr	6	.798	.391291	6	.784	.373750
Third order						
9 variables - . . ., $X_1^2, X_2^3, X_1^2X_2, X_1X_2^2$	7	.852	.337297	7	.771	.387633
10 variables - . . ., $X_1^2, X_2^3, X_1^2X_2, X_1X_2^2$, Zr	7	.886	.296434	7	.861	.302234
Fourth order						
14 variables - $X_1^4, X_2^4, X_1^3X_2, X_1^2X_2, X_1X_2^3$	9	.884	.304932	14	.829	.353575
15 variables - $X_1^4, X_2^4, X_1^3X_2, X_1^2X_2, X_1X_2^3$, Zr	10	.914	.264692	13	.904	.262802

[a]Replication error = 0.072447.

[b]Replication error = 0.096819.

TABLE X. - PARALINEAR CALCULATIONS FROM SPECIFIC WEIGHT CHANGE DATA[a]

[Alloy 1; three samples in three separate runs; temperature, 1200° C.]

Time, hr	Run 1		Run 2		Run 3	
	Input (b)					
	$t_{0\text{-cross}} = 73.77$ $\Delta w/A = -2.71$ mg/cm^2 at t = 200 hr		$t_{0\text{-cross}} = 60.06$ $\Delta w/A = -3.27$ mg/cm^2 at t = 200 hr		$t_{0\text{-cross}} = 33.51$ $\Delta w/A = -3.88$ mg/cm^2 at t = 200 hr	
	$\Delta w/A$, mg/cm^2	w_m/A, mg/cm^2	$\Delta w/A$, mg/cm^2	w_m/A, mg/cm^2	$\Delta w/A$, mg/cm^2	w_m/A, mg/cm^2
1	0.27	0.55	0.26	0.53	0.17	0.37
15	.65	2.25	.56	2.16	.26	1.53
30	.61	3.28	.46	3.15	.06	2.26
45	.45	4.10	.26	3.95	-.21	2.87
60	.23	4.83	0	4.67	-.52	3.41
75	-.02	5.49	-.29	5.32	-.84	3.92
90	-.30	6.11	-.61	5.93	-1.18	4.40
100	-.49	6.50	-.82	6.32	-1.41	4.71
115	-.80	7.07	-1.17	6.88	-1.77	5.16
130	-1.12	7.62	-1.52	7.42	-2.13	5.60
145	-1.45	8.15	-1.88	7.95	-2.50	6.03
160	-1.78	8.66	-2.25	8.47	-2.87	6.46
175	-2.12	9.16	-2.63	8.97	-3.25	6.88
190	-2.47	9.65	-3.01	9.46	-3.63	7.29
200	(c)	9.98	(c)	9.79	(c)	7.56
1000	-23.56	32.25	-25.45	32.92	-24.67	28.54
	Effective thickness change,[d] $10\, w_m/A\left(\frac{\rho_{Ni} + 2\rho_{Al}}{3}\right)$, μm					
200	20.92		20.52		15.86	
1000	67.71		69.01		59.83	

[a]See comparable values in table VIII.

[b]At $\Delta w/A = 0$, $t_{0\text{-cross}} = \left(k_1^{1/2}/k_2\right)^2$; at t = 200 hr, $\Delta w/A = k_1^{1/2}t^{1/2} - k_2 t$.

[c]See Input.

[d]Calculations are for corrosion on one side only.

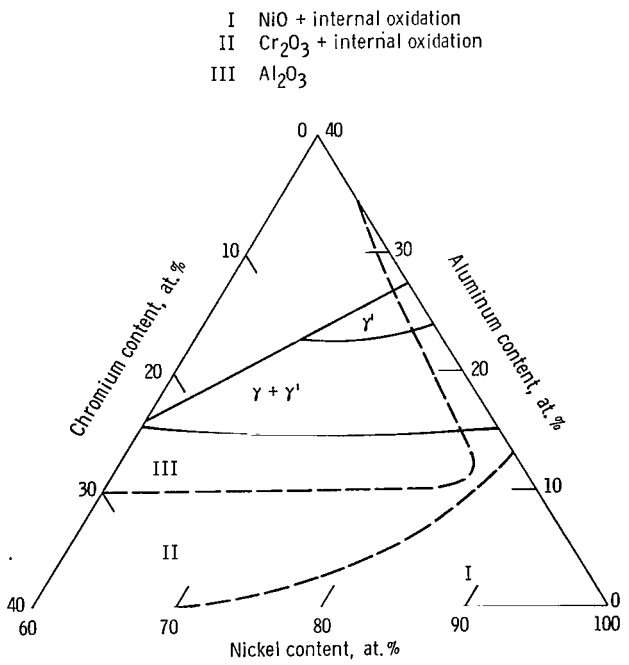

Figure 1. - Oxide map for the ternary system Ni-Cr-Al at 1000° C (ref. 3).

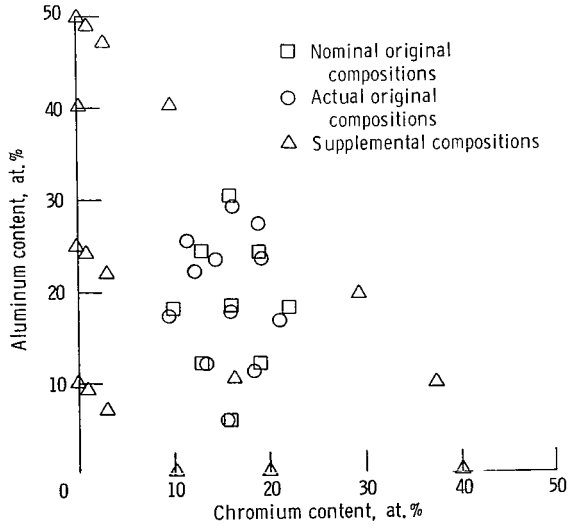

Figure 2. - Distribution of alloy compositions. Balance of all alloys is nickel.

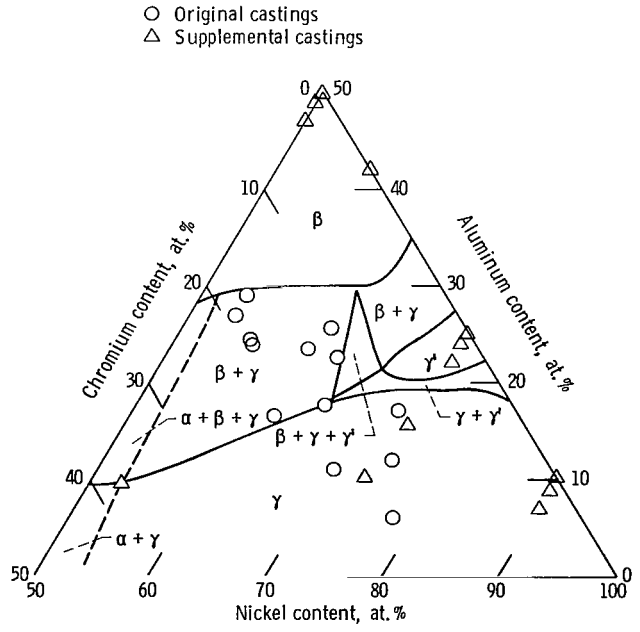

Figure 3. - Distribution of test alloys in Ni-Cr-Al system. Phase diagram at 1200° C after Taylor and Floyd (ref. 7).

(a) Ni-15.81Cr-5.77Al; γ phase.

(b) Ni-9.73Cr-17.18Al; $\gamma + \gamma'$ phase.

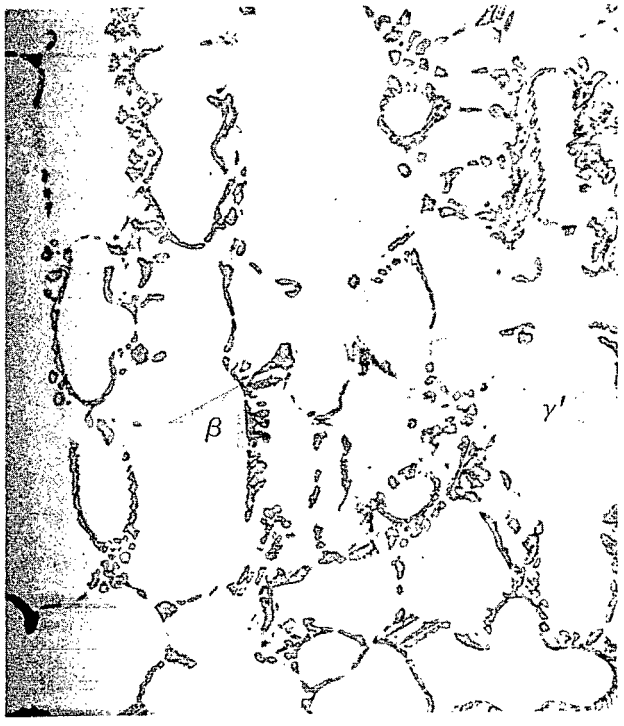

(c) Ni-15.98Cr-17.54Al; $\gamma' + \beta$ phase.

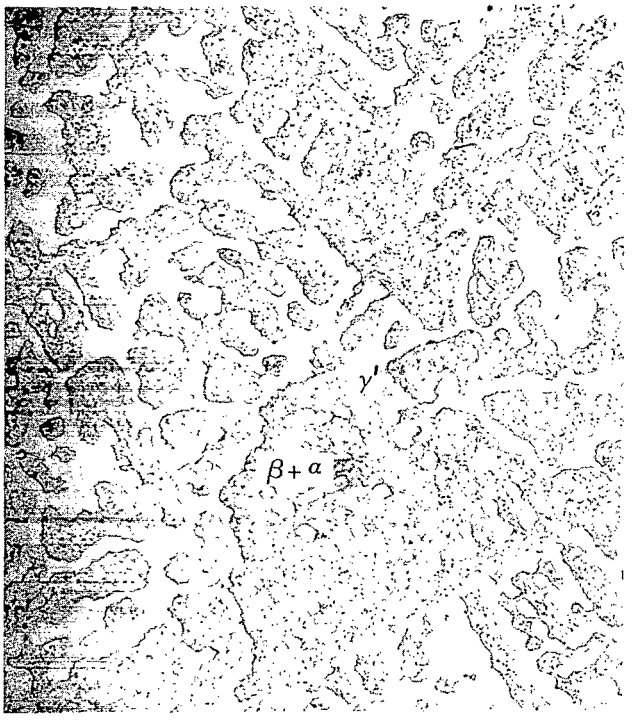

(d) Ni-11.5Cr-25.58Al; $\gamma' + \beta + \alpha$ phase.

Figure 4. - Representative microstructures in Ni-Cr-Al system. Specimens etched; magnification, X250.

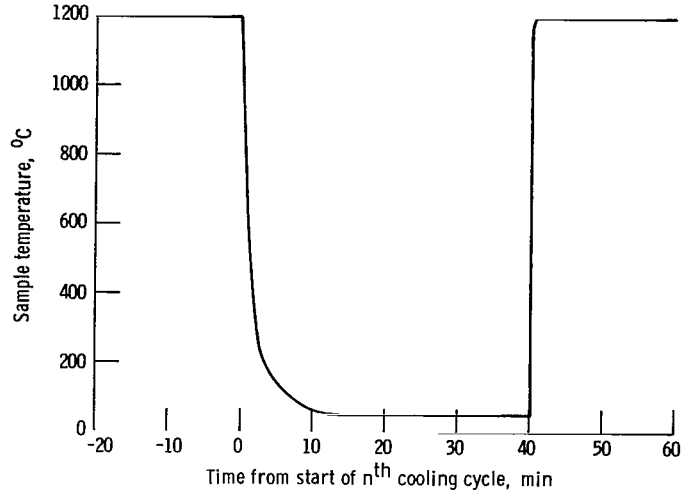

Figure 5. - Temperature profile of typical thermal cycle.

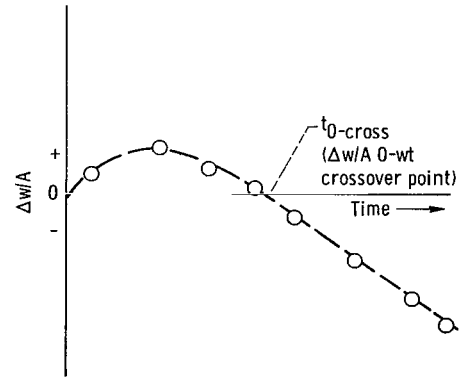

Figure 6. - Typical specific weight change as function of time curve for alloy with nearly uniform scale growth and scale spalling.

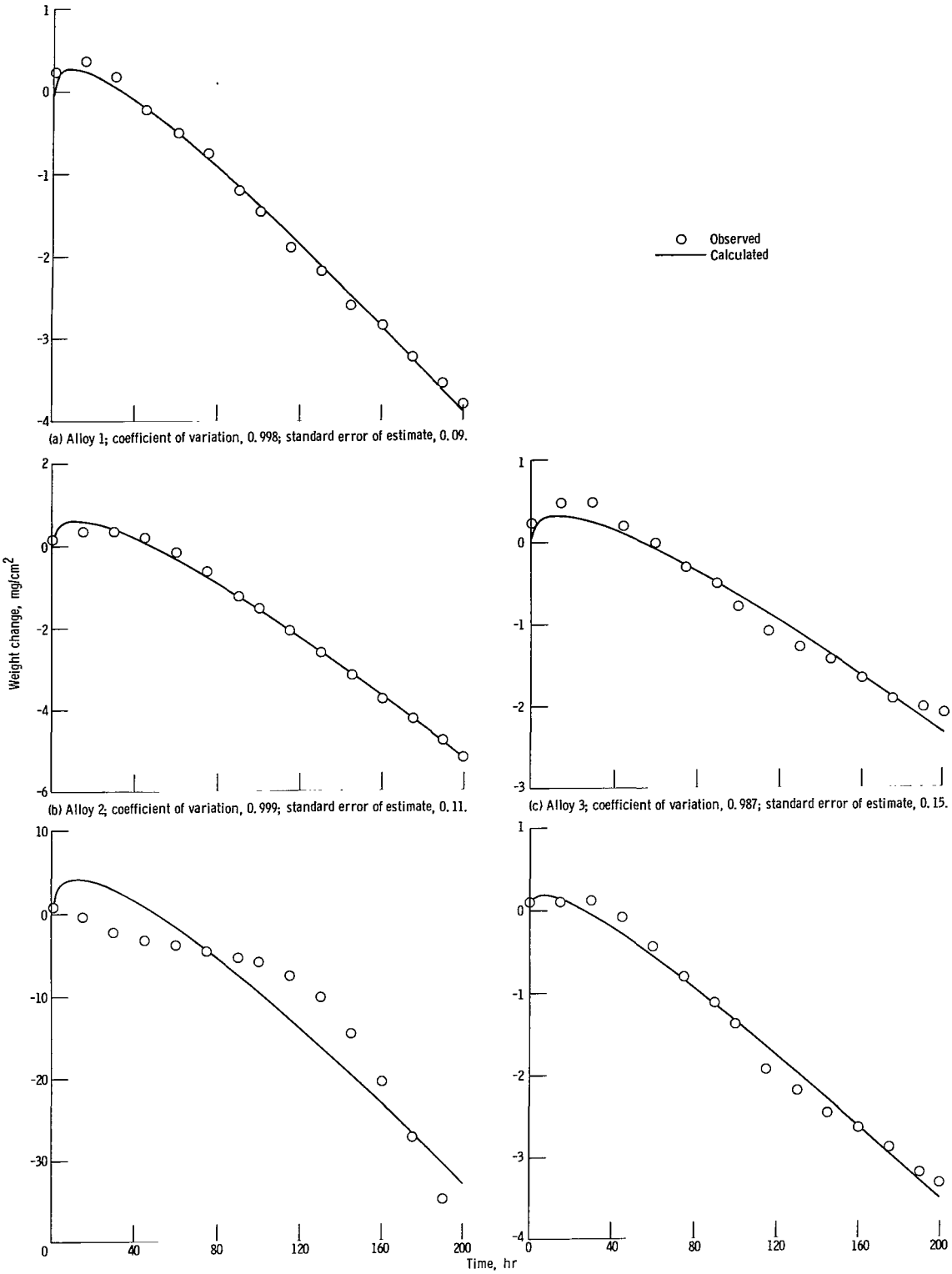

(a) Alloy 1; coefficient of variation, 0.998; standard error of estimate, 0.09.

(b) Alloy 2; coefficient of variation, 0.999; standard error of estimate, 0.11.

(c) Alloy 3; coefficient of variation, 0.987; standard error of estimate, 0.15.

(d) Alloy 7; coefficient of variation, R^2, 0.941; standard error of estimate, σ, 4.52.

(e) Alloy 8; coefficient of variation, 0.995; standard error of estimate, σ, 0.15.

Figure 7. - Comparison of experimental cyclic oxidation data (1200° C, 1-hr cycles) with regression analysis generated expression: $\Delta w/A = K_1^{1/2}t^{1/2} - K_2 t \pm \sigma$.

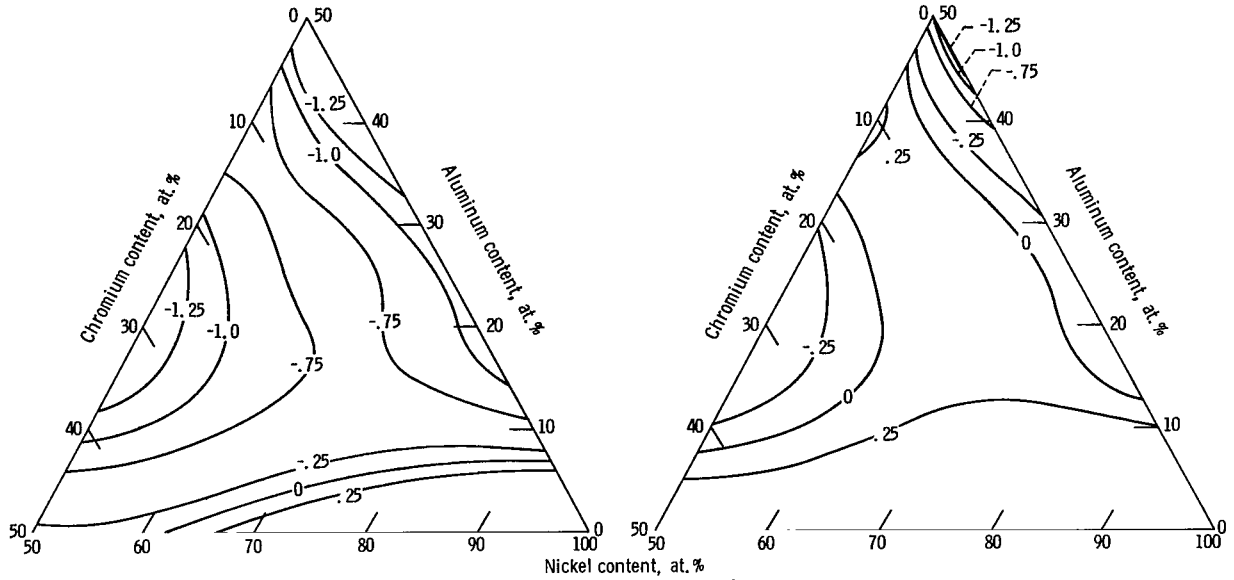

(a) For alloys melted in zirconia crucibles.

(b) For alloys not melted in zirconia crucibles.

Figure 8. - Attack contours in Ni-50Cr-50Al system at 1100° C.

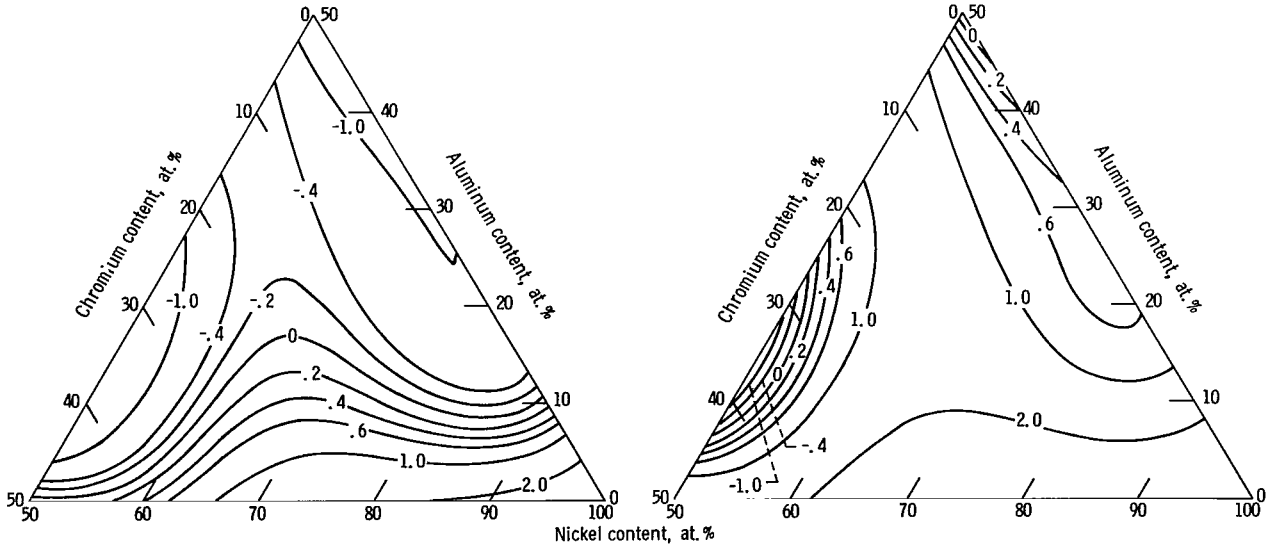

(a) For alloys melted in zirconia crucibles.

(b) For alloys not melted in zirconia crucibles.

Figure 9. - Attack contours in Ni-50Cr-50Al system at 1200° C.

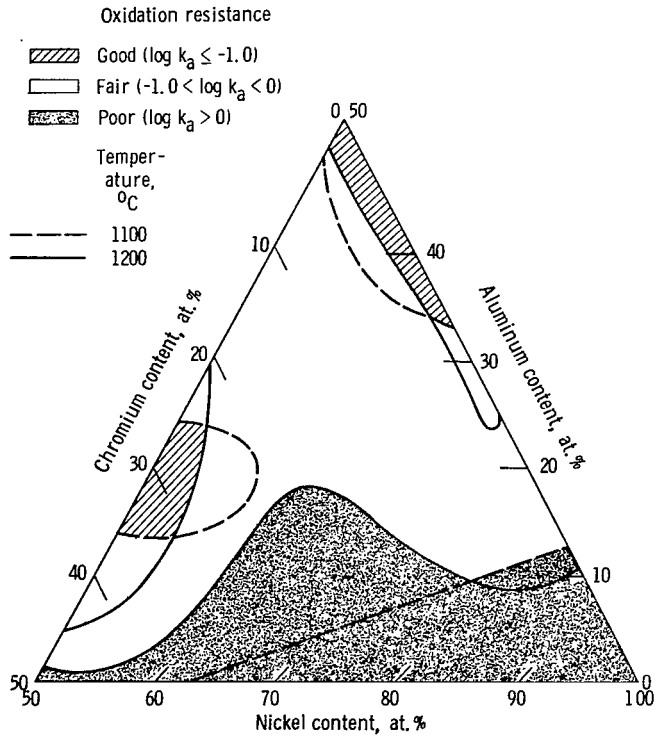

Figure 10. - Overall cyclic oxidation resistance for Ni-Cr-Al alloys at 1100° and 1200° C in still air.

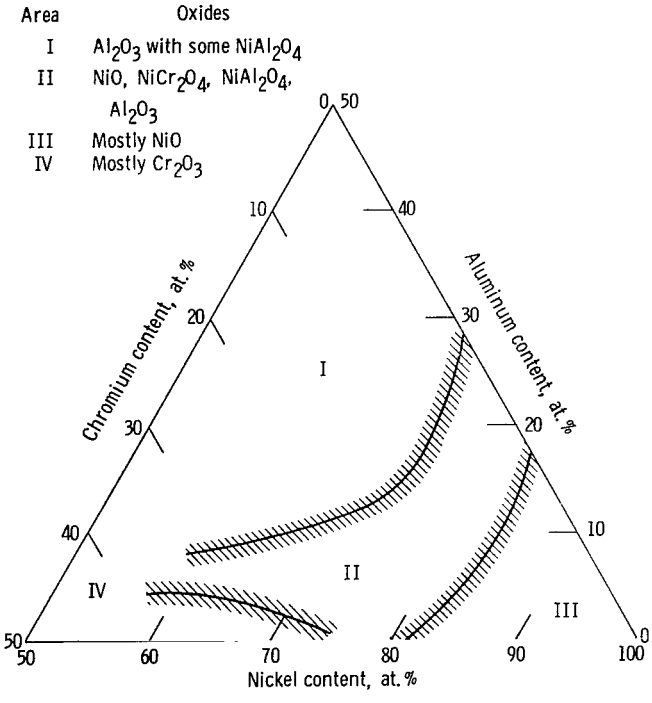

Figure 11. - Oxide map of cyclic oxidation in Ni-Cr-Al system at 1100° and 1200° C.

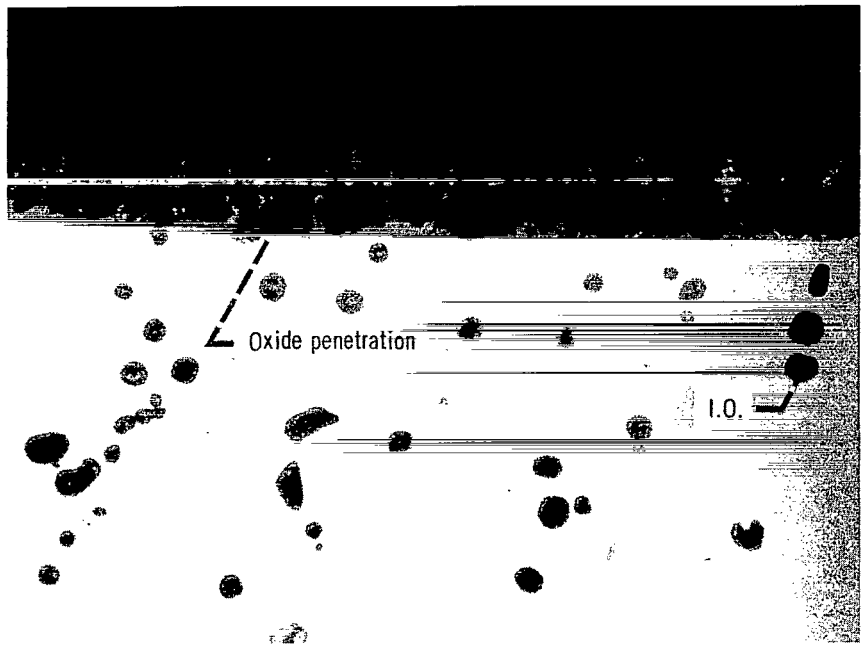

(a) 500 1-hour cycles at 1100° C. X250.

(b) 200 1-hour cycles at 1200° C. X100.

Figure 12. - Internal oxidation and oxide penetration in γ alloy after cyclic oxidation. Etched Ni-15.81Cr-5.77Al.

(a) 500 1-hour cycles at 1100° C. X250.

(b) 200 1-hour cycles at 1200° C. X100.

Figure 13. - Oxide penetration and depletion zone formation in $\gamma + \gamma'$ alloy after cyclic oxidation. Etched Ni-9.73Cr-17.18Al.

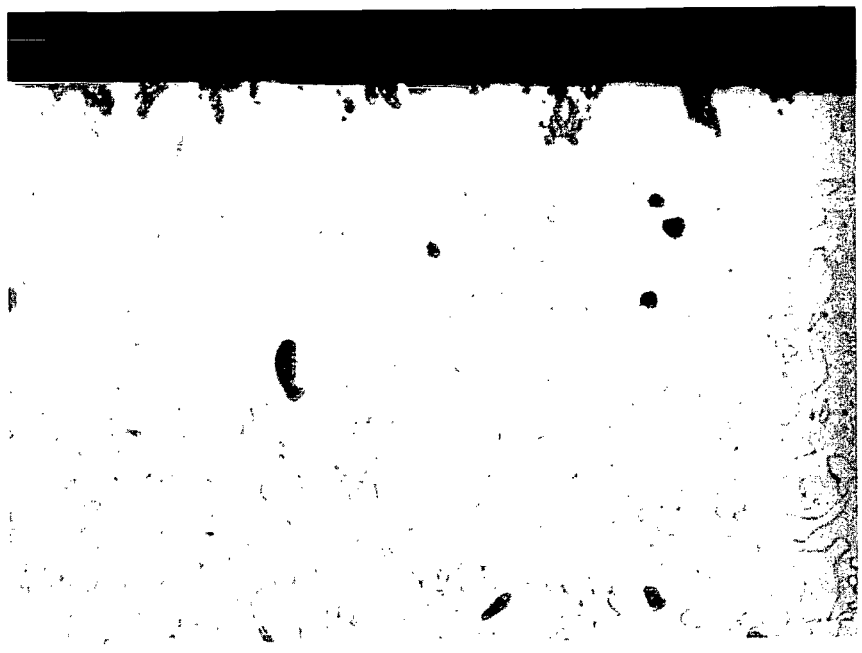

(a) 500 1-hour cycles at 1100° C. X250.

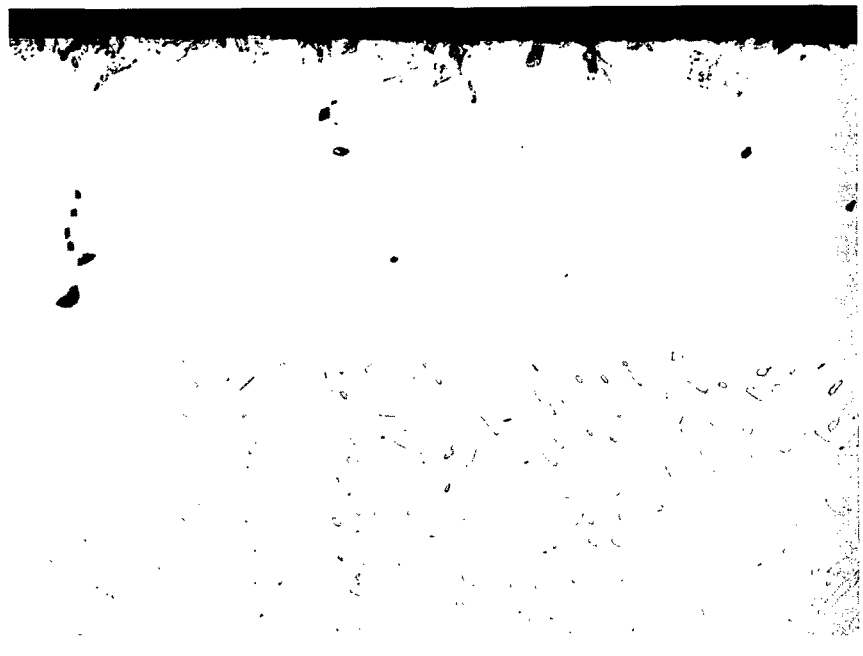

(b) 200 1-hour cycles at 1200° C. X100.

Figure 14. - Depletion zone formation and oxide penetration in $\gamma' + \beta$ alloy during cyclic oxidation. Etched Ni-15.98Cr-17.54Al.

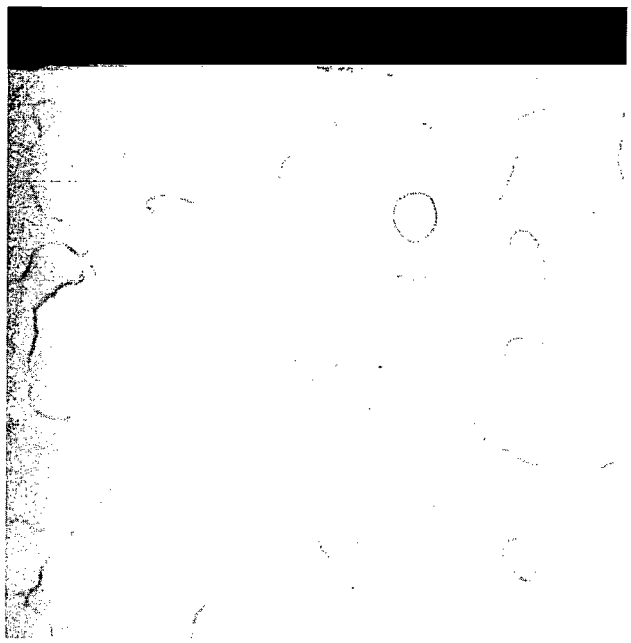

(a) 500 1-hour cycles at 1100° C. X250.

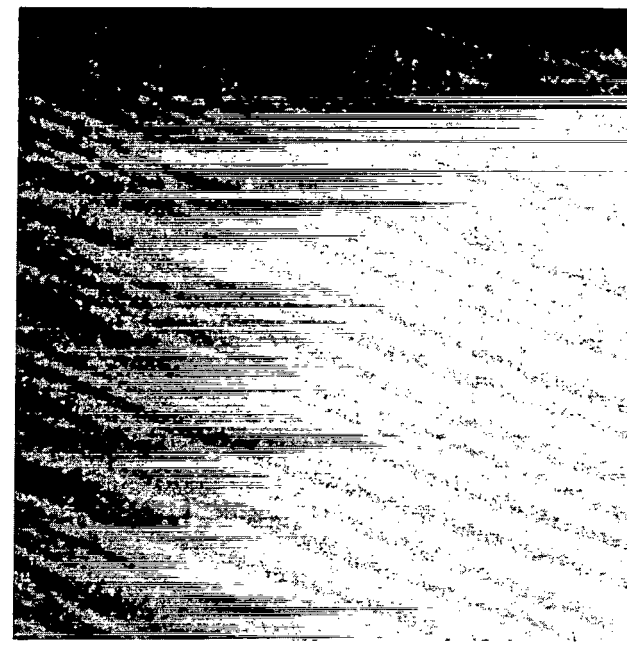

(b) Scanning electron micrograph detail of part (a). X3000.

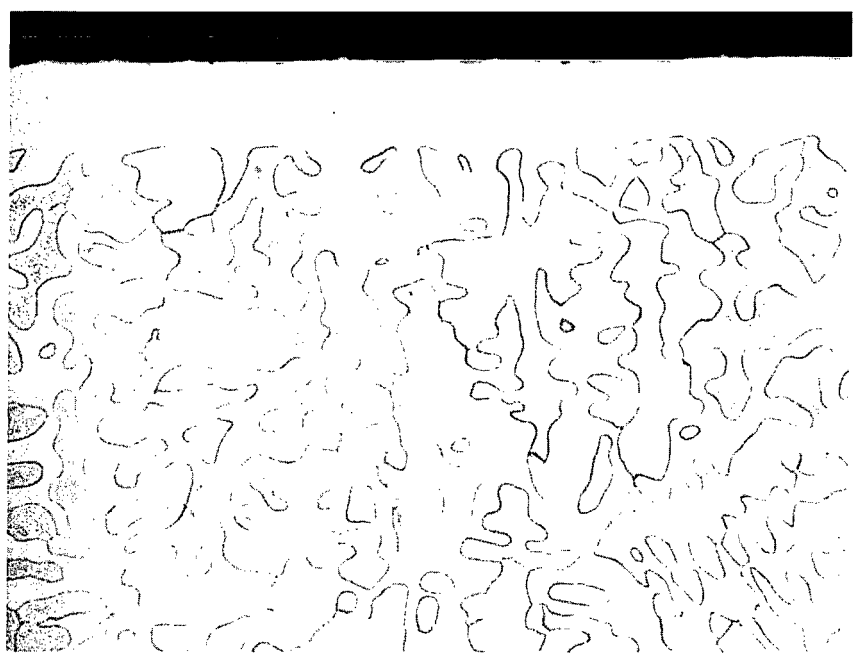

(c) 200 1-hour cycles at 1200° C. X100.

Figure 15. - Depletion zone formation and martensite formation in $\beta + \gamma' + \alpha$ alloy during cyclic oxidation. Etched Ni-11.50Cr-25.58Al.

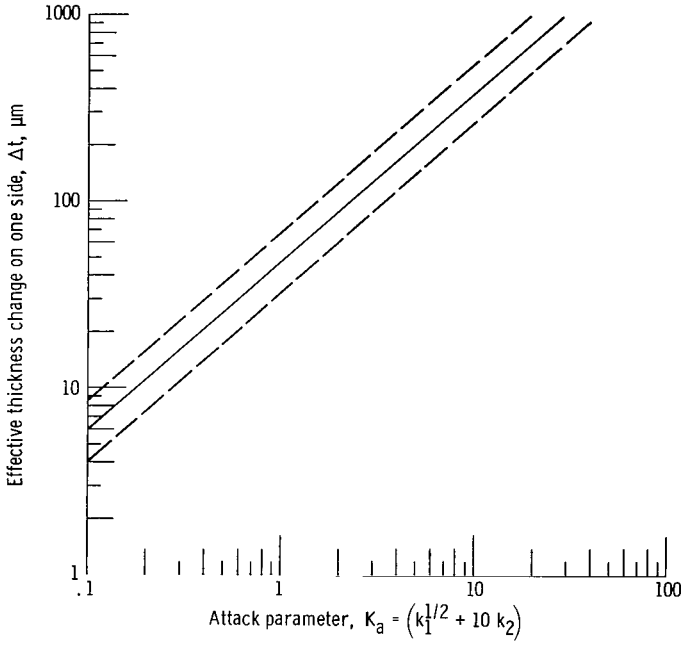

Figure 16. - Correlation of thickness change estimates derived by paralinear analysis and the attack parameter for Ni-Cr-Al alloys forming $NiAl_2O_4$. Derived from 1200^0 C weight change data.

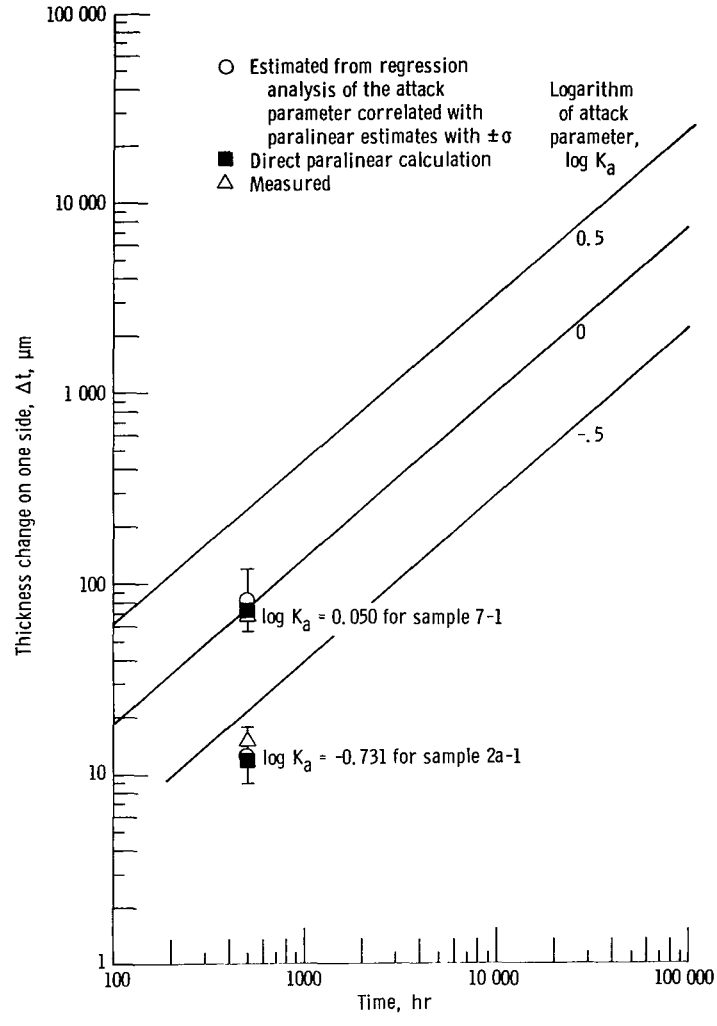

Figure 17. - Estimation of sample thickness change as function of time linking two techniques: paralinear analysis and regression analysis derived from 1200° C data and applied to two samples tested at 1100° C. Based on $NiAl_2O_4$ formation.

NATIONAL AERONAUTICS AND SPACE ADMINISTRATION
WASHINGTON, D.C. 20546

OFFICIAL BUSINESS
PENALTY FOR PRIVATE USE $300

SPECIAL FOURTH-CLASS RATE
BOOK

POSTAGE AND FEES PAID
NATIONAL AERONAUTICS AND
SPACE ADMINISTRATION
451

U.S.MAIL

597 001 C1 U C 760618 S00903DS
DEPT OF THE AIR FORCE
AF WEAPONS LABORATORY
ATTN: TECHNICAL LIBRARY (SUL)
KIRTLAND AFB NM 87117

POSTMASTER: If Undeliverable (Section 158 Postal Manual) Do Not Return

"The aeronautical and space activities of the United States shall be conducted so as to contribute . . . to the expansion of human knowledge of phenomena in the atmosphere and space. The Administration shall provide for the widest practicable and appropriate dissemination of information concerning its activities and the results thereof."

—NATIONAL AERONAUTICS AND SPACE ACT OF 1958

NASA SCIENTIFIC AND TECHNICAL PUBLICATIONS

TECHNICAL REPORTS: Scientific and technical information considered important, complete, and a lasting contribution to existing knowledge.

TECHNICAL NOTES: Information less broad in scope but nevertheless of importance as a contribution to existing knowledge.

TECHNICAL MEMORANDUMS: Information receiving limited distribution because of preliminary data, security classification, or other reasons. Also includes conference proceedings with either limited or unlimited distribution.

CONTRACTOR REPORTS: Scientific and technical information generated under a NASA contract or grant and considered an important contribution to existing knowledge.

TECHNICAL TRANSLATIONS: Information published in a foreign language considered to merit NASA distribution in English.

SPECIAL PUBLICATIONS: Information derived from or of value to NASA activities. Publications include final reports of major projects, monographs, data compilations, handbooks, sourcebooks, and special bibliographies.

TECHNOLOGY UTILIZATION PUBLICATIONS: Information on technology used by NASA that may be of particular interest in commercial and other non-aerospace applications. Publications include Tech Briefs, Technology Utilization Reports and Technology Surveys.

Details on the availability of these publications may be obtained from:

SCIENTIFIC AND TECHNICAL INFORMATION OFFICE

NATIONAL AERONAUTICS AND SPACE ADMINISTRATION

Washington, D.C. 20546